Semiconductor Physics, Quantum Electronics & Optoelectronics, 2011. V. 14, N 2. P. 247-255.

PACS 68.35.bg, 68.37.Tj, 78.20.-e

Structural properties of nanocomposite SiO_2(Si) films obtained by ion-plasma sputtering and thermal annealing

O.L. Bratus', A.A. Evtukh, O.S. Lytvyn, M.V. Voitovych, V.O. Yukhymchuk
V. Lashkaryov Institute of Semiconductor Physics, NAS of Ukraine,
41, prospect Nauky, 03028 Kyiv, Ukraine,
E-mail: bratus1981@ukr.net

Abstract. The nanocomposite SiO_2(Si) films containing Si nanoclusters inside insulating SiO_2 matrix are promising for many nanoelectronics applications. The ion-plasma sputtering of Si in O_2 containing gas mixture and following thermal annealing have been used to form nanocomposite SiO_2(Si) films. The structural properties of the obtained films have been studied using several methods. Among them, there were ellipsometry, IR spectroscopy, Raman spectroscopy, and AFM. Transition of SiO_x matrix into insulating SiO_2 matrix has been revealed by IR spectroscopy. The shift of the transmittance spectra toward high frequency region and the increase in their intensity have been observed. The existence of amorphous and nanocrystalline phases into SiO_2(Si) films have been confirmed using Raman spectroscopy. Two material phases on the film surface, namely SiO_2 and Si, and surface density of silicon nanoclusters have been determined using AFM. It was shown that the size of silicon nanoclusters and their surface density depend on the level of enrichment with silicon of the initial SiO_x film after ion-plasma sputtering and the temperature of subsequent annealing.

Keywords: silicon nanoclusters, nanocomposite films, ion-plasma sputtering, ellipsometry, IR spectroscopy, Raman spectroscopy, AFM.

Manuscript received 14.12.10; accepted for publication 16.03.11; published online 30.06.11.

1. Introduction

Properties of structures with silicon nanoclusters (NC) in dielectric matrix attract great attention for creation of electronic and optoelectronic devices on their basis, namely: light emitting diodes, single-electron transistors and memory cells [1, 2]. The high temperature annealing of silicon enriched silicon oxide (SiO_x) films leads to formation of nanocomposite SiO_2(Si) films. To use these films in electronic devices requires a detailed development of deposition technology and research their properties. The most known technologies for silicon enriched silicon oxide film deposition that intensively used are as follows: plasma enhanced chemical vapor deposition (PECVD) [3-5], low pressure chemical vapor deposition (LPCVD) [6, 7], thermal evaporation in vacuum [8], ion implantation [9], and the simultaneous sputtering of silicon dioxide and silicon [10]. The appearance of silicon inclusions in SiO_2 matrix agrees well with the known process of SiO_x films decomposition on silicon and silicon dioxide phases at high temperatures: $SiO_x \rightarrow ((2-x)/2)Si + (x/2)SiO_2$ [11]. Therefore, studying the phase-structural transformation of SiO_x films has a principal importance for understanding the mechanisms of nanoparticles formation in silicon oxide matrix under thermal annealing.

The method of ion-plasma sputtering (IPS) is suitable to obtain SiO_x films with various silicon concentrations ($0 \le x \le 2$). That gives the opportunity to obtain the nanocomposite SiO_2(Si) films containing Si nanocrystals with different concentration and size. So, the main purpose of this work was to investigate structural properties of nanocomposite SiO_2(Si) films obtained by ion-plasma sputtering for their further use as medium for accumulation and storage of electrical charges in the structures of nonvolatile memory. The influence of silicon content in SiO_x films and annealing temperature on SiO_x films into nanocomposite SiO_2(Si) transformation have been investigated.

© 2011, V. Lashkaryov Institute of Semiconductor Physics, National Academy of Sciences of Ukraine

2. Experimental

The silicon enriched SiO_x films deposited by ion-plasma sputtering and obtained as a result of their high temperature annealing the nanocomposite SiO_2(Si) films were investigated.

Equipment of ion-plasma sputtering (IPS) is designed for deposition of metallic, semiconductor and dielectric films. The design of sputtering part is schematically shown in Fig. 1. It includes the camera (*3*) with a slot diaphragm, tungsten cathode (*2*), and a cooled anode (*1*). There are also the focusing magnetic system (*7*) made from oxide-baric magnets (*6*), ion collector (*5*), and target for sputtering. All items of sputtering part are mounted on the base flanges (*8*). The process of evaporation is as follows: during its operation the heated cathode emits electrons into the cathode space, these moving to the anode ionize the atoms of operation gas (Ar) and create plasma. The negative potential (1–3 kV) in relation to plasma is given on the target. It is enough for plasma discharge appearance and intensive bombardment of targets by positive ions of plasma. The knocked out atoms of target fall on the substrate and deposit on it. Oxygen is inputted into vacuum chamber to obtain the oxides. Sputtered atoms of the target are oxidized on their way and deposited as the oxide on the substrate.

SiO_x films were deposited on polished silicon n-type (100) wafers. The variable parameter was the ratio of gas Ar and O_2 fluxes. Other deposition process parameters were: pressure in the chamber $P = 8\times10^{-4}$ Torr, temperature of substrate T = 150 ºC, current for the cathode heating I_C = 140 A, anode voltage U_A = 50 V, the voltage at the target 1.20-1.25 kV, sputtering current I_S = 0.4 mA. During the ion-plasma sputtering process, partial oxidation of silicon atoms is realized and the proportion of oxidized atoms depends on the O_2/Ar gas ratio.

SiO_x films with different contents of excess silicon were obtained with their thickness in the range 50-60 nm. The content of silicon in the studied samples grew in the sequence N_{Si} (29B) > N_{Si} (29B5) > N_{Si} (29B10) (see Table 1).

To study the effects of annealing temperature on transformation of silicon enriched SiO_x films into nanocomposite SiO_2(Si) films, the annealing at various temperatures (T = 1000, 1050 and 1100 °C) for 30 min in nitrogen atmosphere was performed.

The thickness and refractive index of the films were determined from ellipsometric measurements (λ = 632.8 nm) both after deposition and following thermal annealing.

IR spectra of films were measured within the range $800-1400\,\text{cm}^{-1}$ by using a Fourier spectrometer (Spectrum BX firm Perkin–Elmer). The clean silicon substrate without silicon oxide film was used as the reference one. IR spectra of films were decomposed by Gaussian profiles. Their basic characteristics (position of maximum (ν_M), full width at half maximum (FWHM), area under a band contour (S)) were analyzed in the model of random bonds to determine the molecular

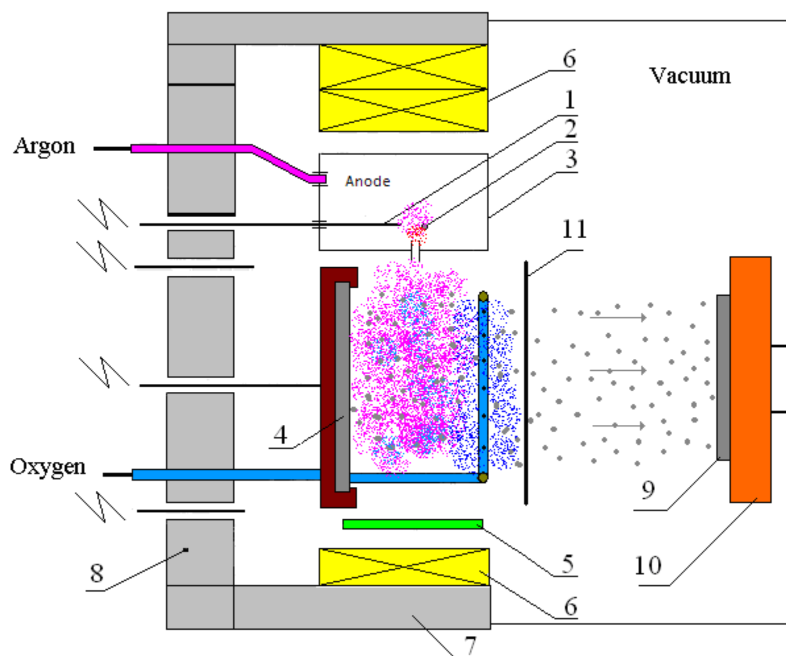

Fig. 1. Schematic image of ion-plasma sputtering set up: *1* – anode, *2* – cathode, *3* – discharge chamber, *4* – target, *5* – collector of ions, *6* – magnets, *7* – magnetic system, *8* – flange, *9* – substrate, *10* – heater, *11* – valve.

© 2011, V. Lashkaryov Institute of Semiconductor Physics, National Academy of Sciences of Ukraine

Table 1. Parameters of the films in dependence on the concentration of silicon content and annealing temperature.

	Annealing temperature, ºC	29B10	29B5	29B
Refractive index, *n*	1000	1.9	–	–
	1050	1.78	1.92	–
	1100	1.76	1.83	1.89
Thickness, nm	1000	54	–	–
	1050	55	53	–
	1100	55	54	51
Nanoclusters height, nm	1000	0.8	–	–
	1050	–	0.3–1.0 /1.0–1.5	–
	1100	1.1	0.4–0.7	1.0–3.0
Nanoclusters density, cm^{-2}	1000	4×10^{10}	–	–
	1050	–	4×10^{10} /1.2×10^{10}	–
	1100	4×10^{10}	8×10^{9}	4×10^{9}
RMS	1000	0.216	–	–
	1050	–	0.315	–
	1100	0.238	0.262	0.353

complexes $\mathrm{Si-O_y-Si_{4-y}}$ $(1 \le y \le 4)$ in structural lattice of SiO_x according to the approach proposed in the paper [12].

Surface morphologies of the films before and after annealing and after etching in 1% solution of HF: H_2O were checked using atomic-force microscope (AFM) of the series NanoScope IIIa in the tapping mode. The silicon probe with nominal edge radius of curvature close to 10 nm was used.

The measurements of Raman spectra of light dispersion were performed at room temperature with a double monochromator DFS-24 in configuration "on reflection". To excite Raman spectra, radiation of Ar^+-laser with the wavelength 514.5 nm was used. The radiation intensity did not exceed 20 mW. Signals were recorded using a cooled photoelectron multiplier in photon-counting mode.

3. Results and discussion

3.1. Ellipsometry. The results of ellipsometric measurements are interpreted as based on the complex refractive index values of the substrate $n_s^* = n_s - ik_s$ and film $n_f^* = n_f - ik_f$, and the film thickness d_f [5]. Thickness and refractive index of SiO_x films in dependence on annealing temperature are presented in Table 1. The growth of refractive index both before and after thermal annealing with increasing the silicon content in the SiO_x film is observed. In a general case, the refractive index may vary with increasing *x* from 3.87 (for silicon) to 1.46 (for SiO_2) [13]. As a result of annealing the initial SiO_x films, the refractive index decreases. The change is larger with growth of annealing temperature (Table 1). It should be noted that in the case of SiO_x films the values of *n* are determined by the composition of oxide (dielectric matrix) [14]. The appearance of areas that contain highly oxidized silicon (with *x* close to two) during the thermal treatment can lead to reduction in the effective refractive index of the film. Increase in the annealing temperature leads to formation of much larger percentage content of highly oxidized silicon. It should reduce the refractive index *n* depending on the increase of the annealing temperature. After high temperature annealing, the nanocomposite films containing Si nanoclusters inside insulating silicon oxide matrix are formed from silicon enriched SiO_x film.

3.2. Infrared spectroscopy. The method of IR spectroscopy allows to characterize the composition and structure of the oxide matrix. The infrared transmission spectra of initial (curve *1*) and annealed at the temperature $T = 1100$ ºC (curve *2*) of silicon oxide films are presented in Fig. 2a. As seen, the main IR absorption band of SiO_x film with the maximum position at $\nu_{M1} = 1026\,\mathrm{cm}^{-1}$ after annealing noticeably shifts to the high frequency region (to $\nu_{M2} = 1076\,\mathrm{cm}^{-1}$), being twice increased in its area. This behavior is mainly associated with the change of phase composition of silicon oxide due to high temperature annealing [15, 16]. It is possible to evaluate the content of deposited SiO_x films from the position of transmission band maximum ν_M for given technology according to the expression [17]:

$$\omega = (987+48.8x)\ \mathrm{cm}^{-1}. \quad (1)$$

© 2011, V. Lashkaryov Institute of Semiconductor Physics, National Academy of Sciences of Ukraine

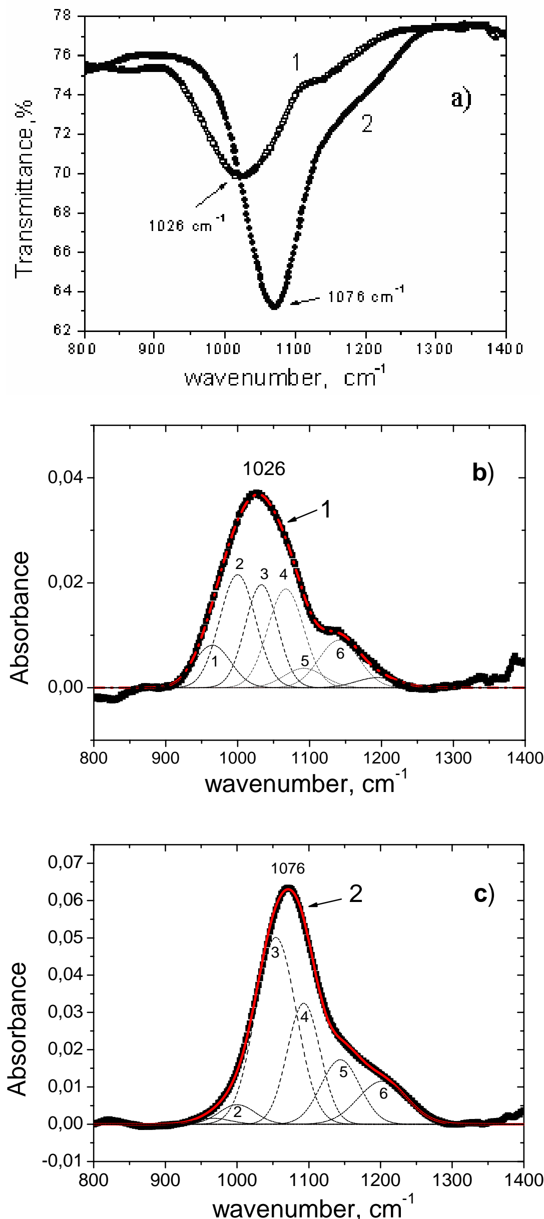

Fig. 2. a) IR transmission spectra of silicon oxide films in the initial (*1*) and annealed (*2*) at T = 1100 ºC for 30 min in N_2 ambient states; b,c) the mathematical deconvolution of the optical density bands of oxide films by Gaussian profile components: before (b) and after annealing (c) (sample 29B).

It was established that the stoichiometry index (x) of the investigated initial SiO_x film was $x \approx 0.8$, while after annealing it became $x \approx 1.82$.

To describe the transformation in the SiO_x structure after the annealing, the IR spectra were rebuilt in the optical density spectra. The optical density spectra of the initial and annealed films with the results of their mathematical decomposition into elementary components with Gaussian profiles, according to the method proposed in [12], are shown in Fig. 2b,c. The parameters of elementary bands (subbands) are adduced in Table 2. As can be seen, the main absorption band of the initial SiO_x film is the sum of seven subbands resulting from transverse (TO mode) and longitudinal (LO mode) valence fluctuations of bridging oxygen that is the part of the molecular complexes $Si-O_y-Si_{4-y}$ ($1 \le y \le 4$). The main contribution to the IR absorption band of initial film is given by the subbands 2, 3, 4, which correspond to complexes of unoxidized silicon ($Si-O-Si_3$, $Si-O_2-Si_2$, $Si-O_3-Si$). The contribution of subband 5 (SiO_4) in the total area of the band is negligible. Subbands 6 and 7 are associated with longitudinal fluctuations of valence (LO) $Si-O$ bond. As a result of annealing the initial silicon enriched SiO_x ($x \approx 0.8$) film, its transformation into the film SiO_x with stoichiometry index $x \approx 1.82$ is realized, and redistribution of intensities of elementary bands (Fig. 2c, Table 2) is observed. The integral intensity of the subband associated with $Si-O-Si_3$ complexes decreases by 6.5 times, and subbands associated with the $Si-O_2-Si_2$, $Si-O_3-Si$ complexes disappear. The relative area of subbands caused by $Si-O$ TO vibration modes from the SiO_4 tetrahedron combined into 4- and 6-fold rings is approximately 68%, and the area of $Si-O-Si$ subband is 14.6% of the total spectrum area indicating formation of SiO_2 phase regions.

The $Si-O-Si_3$ complexes are present in the film after heat treatment (Table 2). It indicates incomplete phase separation caused by annealing. This means the existence of SiO_x phase that is associated by us with a transition layer between Si nanoparticles and SiO_2 matrix.

For a complete description of the spectra, the band $965\,cm^{-1}$ was also used. It is caused by $Si-O-Si$ complexes in $a\text{-}Si:H$ [12]. Its appearance in the initial SiO_x film relates to the presence of water vapor or hydrogen in the operation gas during deposition.

Thus, the heat treatment of SiO_x films causes decay of molecular complexes of weakly oxidized silicon and promotes formation of Si clusters and heavily oxidized silicon dioxide matrix.

3.3. Surface morphology. Atomic-force microscopy (AFM) was used to analyze the structure of surface. The AFM morphology image of the initial SiO_x film obtained by ion-plasma sputtering is shown in Fig. 3a. It is sufficiently homogeneous surface (RMS ≈ 0.18 nm) formed with small grains of up to 0.4 nm height. As a result of high temperature annealing at T = 1000 and 1100 ºC for 30 min (sample 29B10), surface morphology changes with appearance of nanoinclusions (Fig. 3b,c). Annealing at the temperature 1000 ºC stimulated formation of nanoislands of 0.8 nm height with their surface density of $N \approx 4 \times 10^{10}\,cm^{-2}$. After higher annealing temperature (1100 ºC), the density of islands did not change, but their height was increased up to 1.1 nm.

© 2011, V. Lashkaryov Institute of Semiconductor Physics, National Academy of Sciences of Ukraine

Table 2. Parameters of elementary absorption subbands of SiO_x films before and after thermal annealing.

Sample	Subband	Maximum position, cm^{-1}	Vibration mode	Component of structure	Subband area (normalized on full area of band for TO and LO vibrations, respectively)
SiO_x (29A) before annealing	1	965		Si–O–Si in a-Si:H	9.9
	2	1000	TO	$Si–O–Si_3$	26.22
	3	1033	TO	$Si–O_2–Si_2$	21.36
	4	1067	TO	$Si–O_3–Si$	22.72
	5	1092	TO	$Si–O_4$	4.85
	6	1141	LO	$Si–O–Si_3$	12.23
	7	1195	LO	$Si–O_2–Si_2$	2.72
	Maximum position of absorption band, cm^{-1}				**1026, x = 0.8**
SiO_2(Si) (29B) after annealing	1	965	TO	Si–O–Si in a-Si:H	1.25
	2	1000	TO	$Si–O–Si_3$	4
	3	1054	TO	4-fold ring of SiO_4	44.64
	4	1093	TO	4 and 6-fold ring of SiO_4	23.30
	5	1144	TO	Si–O–Si β-crystobalite	14.6
	6	1203	LO	4-fold ring of SiO_4	12.21
	Maximum position of absorption band, cm^{-1}				**1076, x = 1.82**

The behavior of the sample 29B5 with growth of annealing temperature is shown in Fig. 4a. Annealing at T = 1050 ºC leads to formation of nanoislands of two types on the surface, namely: the smaller ones with 0.3-1.0 nm height and surface density of $N \approx 4\times10^{10}$ cm^{-2} and higher ones with 1.0-1.5 nm height and density of 1.2×10^{10} cm^{-2}. The higher annealing temperature T = 1100 ºC leads to formation of homogeneous, but wider nanoislands. Their height decreased down to 0.4-0.7 nm. There is also a significant reduction in the nanoisland density ($N \approx 8\times10^{9}$ cm^{-2}).

The AFM image of the sample 29B that was annealed at T = 1100 ºC for 30 min in a nitrogen ambient is presented in Fig. 5a (scale height is 20 nm). As seen from this figure, the height of nanoinclusions lies within 2.1-2.6 nm, and the RMS is 0.35 nm.

The periodic contact mode, in which AFM measurements were carried out, simultaneously with the topography, allows to register the shift in the phase of probe fluctuations. In our case, it confirmed the presence of two phases on the sample 29B5 surface (Fig. 4c,d). This shift may be caused by two factors: (i) sharp changes in height on the probe way or (ii) local changes of the surface properties (adhesion, elasticity, hardness), where, in their turn, are caused by changing the chemical composition. In the first case, the sign of the shift will be varied during the pass of three points: horizontally-sharply up, top-down (top), sharply down-horizontally. In the second one, the sign of the shift will be varied only during the passage over two points in the transition from the basic structure of this surface to a local island with the other content and back. One can see that, in our case, the phase shift is caused by the second factor. Thus, it can be assumed that the islands have another chemical composition than that of the main surface.

The visual increase in the lateral size of nanoislands is explained by the broadening effect of AFM topographic images, which depends on the radius of curvature of the probe top. The value of instrumentation broadening at AFM registration of nanoislands is described by the expression $L_{spread} = 2\,(2R\times h)^{0.5}$ [9], where R is the radius of

© 2011, V. Lashkaryov Institute of Semiconductor Physics, National Academy of Sciences of Ukraine

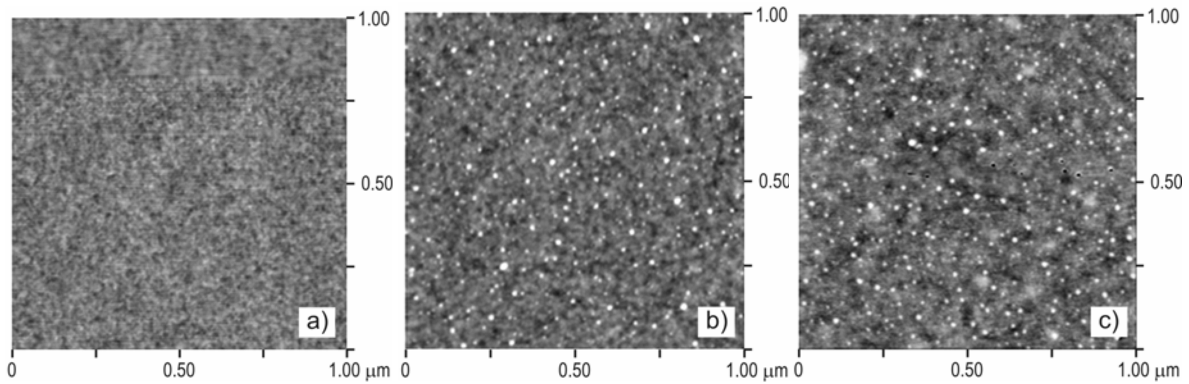

Fig. 3. AFM images of film surfaces (sample 29B10): initial SiO_x (a); annealed at temperatures 1000 ºC (b) and 1100 ºC (c).

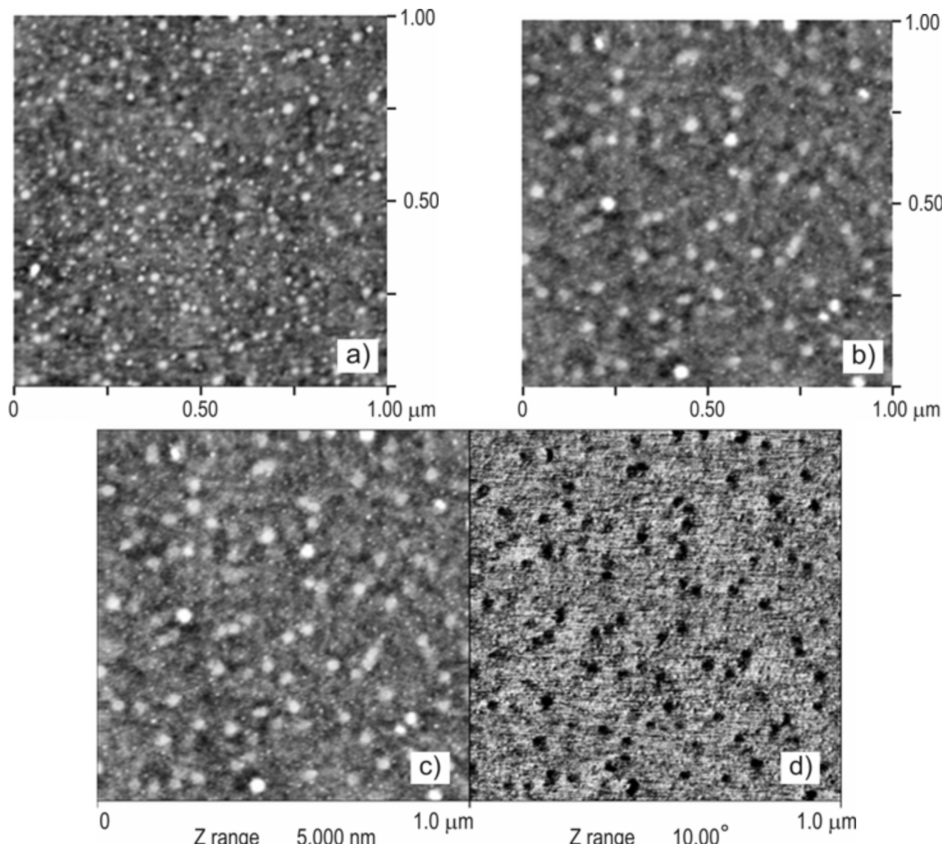

Fig. 4. AFM images of film surfaces (sample 29B5) after annealing at temperatures: a) 1050 ºC, b) 1100 ºC and c, d) topography and phase-change map of probe vibrations for annealed at T = 1100 ºC film, respectively.

curvature of the probe top (R = 10 nm in our case), h is the height of nanoisland.

Thus, the thermal annealing led to formation of the nanoislands with other chemical composition, namely, silicon on the background of the original surface [18, 19]. Comparing the influence of the quantity of enriched silicon in initial SiO_x films on formation of relief due to the high temperature annealing, it is possible to conclude that the higher concentration of silicon in the initial films the larger islands are formed, but their density decreases.

3.4. Etching. The fact that annealing of SiO_x film results in formation of nanocomposite SiO_2 (Si) film was evidenced by analysis of IR spectra, AFM images and measurements in the periodic contact mode, and it can be also demonstrated when processing the sample surface by etching in water solution of hydrofluoric acid. The same procedure was earlier performed for layers of SiO_x obtained by thermal vacuum evaporation [8], PECVD [20] and ion implantation [9] methods. For this purpose, we etched the surface of annealing film in 1% solution of HF:H_2O. After etching the sample 29B (with

© 2011, V. Lashkaryov Institute of Semiconductor Physics, National Academy of Sciences of Ukraine

the highest content of excess silicon, which was annealed at $T = 1100$ °C for 30 min in a nitrogen ambient), the film thickness decreased by 6 nm and became 45 nm. The analysis of Fig. 5b shows that the RMS was increased from 0.35 nm up to 1.43 nm, and the height of nanocrystals increased from 2.1-2.6 nm to 9-10 nm. This change of the nanocrystal height is consistent with measurements of the film thickness before and after etching as observed using ellipsometry.

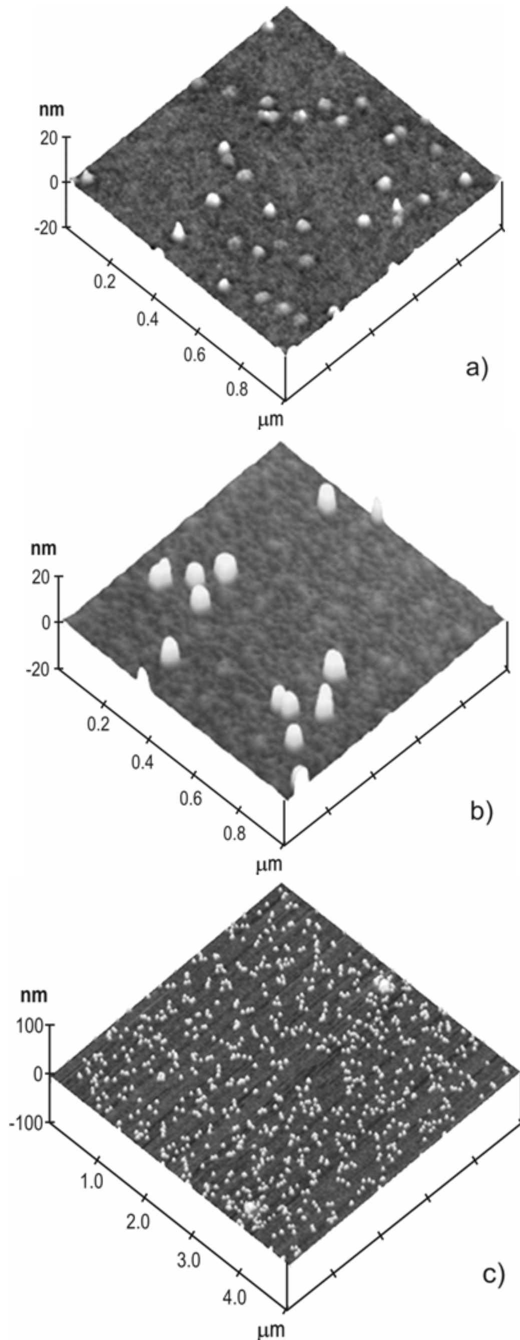

Fig. 5. AFM images of nanocomposite $SiO_2(Si)$ film (sample 29B): a) before and b) after treatment in acid solution; c) a piece of the sample surface with the area 5×5 µm after processing.

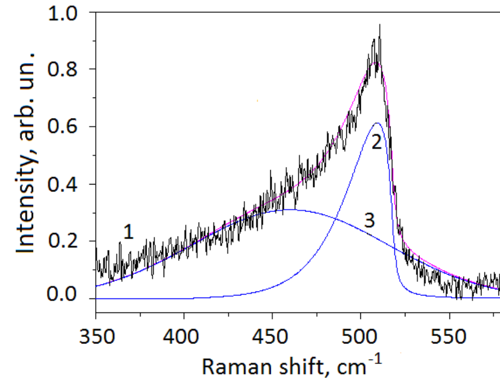

Fig. 6. Experimental Raman spectrum of the investigated film in Si – Si vibrations region (*1*) and theoretical curves that describe the contribution to the spectra of nanocrystalline (*2*) and amorphous (*3*) phases.

To determine the surface density and uniformity of nanocrystals distribution after processing in a solution of HF:H_2O, the AFM image with larger sizes 5×5 µm (Fig. 5c) has been made. The analysis of this figure shows that nanocrystals are distributed on the plate almost homogeneous, but disordered. To take into account that the solution of hydrofluoric acid does not dissolve the silicon, poorly dissolves non-stoichiometric oxide ($x < 2$) and well dissolves the silicon dioxide, it is possible to conclude that the given results clearly demonstrate the phase transformation and formation of silicon nanocrystals in the SiO_2 matrix after thermal annealing.

The obtained experimental results are in accordance with the literature data concerning formation of silicon nanocrystals after annealing of silicon enriched SiO_x films and confirmed by transmission electron microscope images [21, 22].

3.5. Raman spectra. The Raman spectrum of investigated films within the range of Si – Si vibrations is shown in Fig. 6. As seen, this experimental spectrum consists of two bands corresponding to amorphous and nanocrystalline silicon. To determine the parameters of composite bands, the experimental spectrum was decomposed by Gaussian curves that described the band of amorphous phase and asymmetric curve that described the contribution of the nanocrystals. The latter has a view [23, 24]:

$$I(\nu) = \int \exp\left(-\frac{q^2 D^2}{16\pi^2}\right) \frac{d^3 q}{(\nu - \nu(q))^2 + (\Gamma_0 / 2)^2}\,, \qquad (2)$$

where Γ_0 is the halfwidth of the phonon band for Si single crystal, $\nu(q)$ is the dispersion dependence. As determined from this schedule, the frequencies of bands were obtained from spectral decomposition and are $462\,\mathrm{cm}^{-1}$ and $508.5\,\mathrm{cm}^{-1}$, correspondingly. The frequency band position of $508.5\,\mathrm{cm}^{-1}$ corresponds to

© 2011, V. Lashkaryov Institute of Semiconductor Physics, National Academy of Sciences of Ukraine

the nanocrystals with an average size of 2.7 nm according to the model proposed in the paper [24]. It is necessary to take into account that there are some distribution of silicon nanocrystal sizes and amorphous phase in the investigated film, which cause an error in experimental curve description and, correspondingly, when determining the average nanocrystal size.

4. Conclusions

It was shown that thermal annealing of silicon enriched SiO_x films leads to formation of Si nanoclusters into the matrix of strongly oxidized silicon dioxide.

The size of silicon nanoclusters and their surface density depend on the level of enrichment of the initial SiO_x film with silicon and a subsequent annealing temperature.

Processing the nanocomposite SiO_2(Si) film in a water solution of hydrofluoric acid clearly demonstrates the phase transformation and formation of silicon nanocrystals inside the SiO_2 matrix after thermal annealing.

So, the method of ion-plasma sputtering allows to obtain the enriched with silicon SiO_x film that after high temperature annealing is transformed into the nanocomposite SiO_2(Si) film containing Si nanoclusters in dielectric matrix.

Acknowledgements

This work was supported in part by National Academy of Sciences of Ukraine under Projects #52 and #41. We thank Prof. V. Litovchenko for useful discussions.

References

1. H.I. Hanafi, S. Tiwari, and I. Khan, Fast and long retention-time nanocrystal memory // *IEEE Trans. Electron. Devices*, **43**, p. 1553-1558 (1996).
2. S. Tiwari, F. Rana, H. Hanafi, A. Hartstein, E.F. Crabbe, K. Chan, A silicon nanocrystals based memory // *Appl. Phys. Lett.* **68**, №10, p. 1377-1379 (1996).
3. X.Y. Chen, Y.F. Lu, Y.H. Wu, B.J. Cho, L.J. Tang, D. Lu, J.R. Dong, Correlation between optical properties and Si nanocrystal formation of Si-rich Si oxide films prepared by plasma-enhanced chemical vapor deposition // *Appl. Surf. Sci.* **253**, p. 2718-2726 (2006).
4. N. Daldosso, G. Das, S. Larcheri, G. Mariotto, G. Dalba, and L. Pavesi, Silicon nanocrystal formation in annealed silicon-rich silicon oxide films prepared by plasma enhanced chemical vapor deposition // *J. Appl. Phys.* **101**, 113510 (2007).
5. O.L. Bratus’, T. Gorbanyuk, A.A. Evtukh, V. Litovchenko, Ye. Pakhlov, Properties of SiO_x and SiO_2(Si) nanocomposite films prepared by the PECVD method // *Collection of scientific papers “Nanosystems, nanomaterials, nanotechnologies”*, **5** (1), p. 135-147 (2007).
6. M. Ivanda, H. Gebavi, D. Ristic, K. Furic, S. Music, M. Ristic, S. Zonja, P. Biljanovic, O. Gamulin, M. Balarin, M. Montagna, M. Ferarri, G.C. Righini, Silicon nanocrystals after thermal annealing of Si-rich silicon-oxide prepared by the LPCVD method // *J. Molecular Structure* **834-836**, p. 461-464 (2007).
7. V. Turchanikov, A. Nazarov, V. Lysenko, E. Tsoi, A. Salonidou, A.G. Nassiopoulou, Charging/dis-charging kinetics in LPCVD silicon nanocrystal MOS memory structures // *Physica E* **38**, p. 89-93 (2007).
8. I.P. Lisovskii, I.Z. Indutnyi, B.N. Gnennyi et al., Phase-structure transformations in the SiO_x films during vacuum thermoannealing // *Fizika tekhnika poluprovodnikov*, **37**(1), p. 98-103 (2003), in Russian.
9. M.S. Dunaevskii, J.J. Grob, A.G. Zabrodskii, R. Laiho, A.M. Titkov, AFM visualization of Si nanocrystals in thermal oxide SiO_2 by using selective etching // *Fizika tekhnika poluprovodnikov*, **38**(11), p. 1294-1300 (2004), in Russian.
10. I.V. Antonova, M.B. Guliaev, Z.Sh. Yanovitskaya, V.A. Volodin, D.V. Marin, M.D. Yefremov, Y. Goldstein, J. Jedrzejewski, Juxtaposition of electric properties and photoluminescence depending on content of SiO_x layers with silicon nanocrystals // *Fizika tekhnika poluprovodnikov*, **40**(10), (2006), in Russian.
11. Y.C. Fang, Z.J. Zhang, M. Lu, Room temperature photoluminescence mechanism of SiO_x film after annealing at different temperatures // *J. Luminescence*, **126**, p. 145-148 (2007).
12. I.P. Lisovskii, V.G. Litovchenko, V.B. Lozinskii, S.I. Frolov, H. Flietner, W. Fussel, E. Schmidt, IR study of short-range and local order in SiO_2 and SiO_x films // *J. Non-Cryst. Solids* **187**, p. 91 (1995).
13. A.A. Evtukh, I.P. Lisovskii, V.G. Litovchenko, A.Yu. Kizjak, Yu.M. Pedchenko, L.I. Samotovka, Study of the structure of ultrathin silicon dioxide films // *Ukr. J. Phys.* **51**(3), p. 296-304 (2006).
14. W.Y. Ching, Theory of amorphous SiO_2 and SiO_x. I. Atomic structural models // *Phys. Rev. B*, **26**(12), p. 6610-6621 (1982).
15. K. Hubner, Chemical bond and related properties of SiO_2. VII. Structure and electronic properties of the SiO_x region of Si-SiO_2 interfaces // *Phys. status solidi* (*a*), **61**(2), p. 665 (1980).
16. M. Nakamura, Y. Mochizuki, K. Usami, Y. Itoh, T. Nozaki, Infrared absorption spectra and compositions of evaporated silicon oxides (SiO_x) // *Solid State Communs*. **50**, p. 1079 (1984).
17. Z.X. Ma, X.B. Liao, J. He, W.C. Cheng, G.Z. Yue, Y.Q. Wang, G.L. Kong, Annealing behaviors of photoluminescence from SiO_x:H // *J. Appl. Phys.* **83**, p. 7934-7939 (1998).

© 2011, V. Lashkaryov Institute of Semiconductor Physics, National Academy of Sciences of Ukraine

18. M.A. Salem, H. Mizuta, and S. Oda, Probing electron charging in nanocrystalline Si dots using Kelvin probe force microscopy // *Appl. Phys. Lett*. **85**(15), 11 October 2004.
19. S. Oda, S.Y. Huang, M.A. Salem, D. Hippo, H. Mizuta, Charge storage and electron/light emission properties of silicon nanocrystals // *Physica E*, **38**, p. 59-63 (2007).
20. A. Evtukh, O. Bratus', T. Gorbanyuk, and V. Ievtukh, Electrical characterization of SiO_2(Si) films as a medium for charge storage // *Phys. status solidi* (*c*), **5**, No.12, p. 3663-3666 (2008).
21. T. Inokuma Y. Wakayama, T. Muramoto, R. Aoki, Y. Kurata, and S. Hasegawa, Optical properties of Si clusters and Si nanocrystallites in high-temperature annealed SiO_x films // *J. Appl. Phys*. **83**, No.4, p. 2228 (1998).
22. Y.Q. Wang, R. Smirani, G.G. Ross, The formation mechanism of Si nanocrystals in SiO_2 // *J. Cryst. Growth* **294**, p. 486-489 (2006).
23. H. Richter *et al.* // *Solid State Communs.* **39**, p. 625 (1981).
24. H. Cambell and P. Fauchet // *Solid State Communs*. **58**, p. 739 (1986).

© 2011, V. Lashkaryov Institute of Semiconductor Physics, National Academy of Sciences of Ukraine